Inorg. Chem. **2006**, *45*, 4526–4536

Spectral and Structural Characterization of Amidate-Bridged Platinum–Thallium Complexes with Strong Metal–Metal Bonds

Wanzhi Chen,*[,†] Fenghui Liu,[†] Kazuko Matsumoto,*[,‡] Jochen Autschbach,*[,§] Boris Le Guennic,[§] Tom Ziegler,[||] Mikhail Maliarik,[⊥] and Julius Glaser[#]

Department of Chemistry, Zhejiang University, Hangzhou 310028, China, Department of Chemistry, Advanced Research Institute for Science and Engineering, Waseda University, Okubo 3-4-1, Shinjuku Ku, Tokyo, Japan, Department of Chemistry, University at Buffalo, State University of New York, 312 Natural Sciences Complex, Buffalo, New York 14260-3000, Department of Chemistry, University of Calgary, Calgary, Alberta, Canada T2N 1N4, IFM, Department of Chemistry, Linköping University, SE-581 83 Linköping, Sweden, and Department of Chemistry, Royal Institute of Technology (KTH), S-100 44 Stockholm, Sweden

Received September 29, 2005

The reactions of $[Pt(NH_3)_2(NHCO^tBu)_2]$ and TlX_3 ($X = NO_3^-$, Cl^-, $CF_3CO_2^-$) yielded dinuclear $[\{Pt(ONO_2)(NH_3)_2(NHCO^tBu)\}Tl(ONO_2)_2(MeOH)]$ (**2**) and trinuclear complexes $[\{PtX(RNH_2)_2(NHCO^tBu)_2\}_2Tl]^+$ [$X = NO_3^-$ (**3**), Cl^- (**5**), $CF_3CO_2^-$ (**6**)], which were spectroscopically and structurally characterized. Strong Pt–Tl interaction in the complexes in solutions was indicated by both ^{195}Pt and ^{205}Tl NMR spectra, which exhibit very large one-bond spin–spin coupling constants between the heteronuclei ($^1J_{PtTl}$), 146.8 and 88.84 kHz for **2** and **3**, respectively. Both the X-ray photoelectron spectra and the ^{195}Pt chemical shifts reveal that the complexes have Pt centers whose oxidation states are close to that of Pt^{III}. Characterization of these complexes by X-ray diffraction analysis confirms that the Pt and Tl atoms are held together by very short Pt–Tl bonds and are supported by the bridging amidate ligands. The Pt–Tl bonds are shorter than 2.6 Å, indicating a strong metal–metal attraction between these two metals. Compound **2** was found to activate the C–H bond of acetone to yield a platinum(IV) acetonate complex. This reactivity corresponds to the property of Pt^{III} complexes. Density functional theory calculations were able to reproduce the large magnitude of the metal–metal spin–spin coupling constants. The couplings are sensitive to the computational model because of a delicate balance of metal 6s contributions in the frontier orbitals. The computational analysis reveals the role of the axial ligands in the magnitude of the coupling constants.

Introduction

The bonding interactions between closed-shell, heavy-metal ions is gaining increasing attention because the complexes containing such metal−metal attractive interactions display unique physical and chemical properties and are potentially applicable as electronic conductors, photosensitizers, and photocatalysts for solar photochemical energy conversion.[1] A number of metal complexes and coordination polymers with Au−Au, Au−Tl, and Au−Ag interactions have been experimentally and theoretically studied in recent years. In the case of Pt, many examples of heteronuclear complexes with other closed-shell metal ions have been reported, for example, Cu^I,[2] Ag^I,[2] Pb^{II},[3] Hg^{II},[4] Cd^{II},[5] Tl^I,[6,7] and Tl^{II},[8] giving rise to materials in which the metal−metal separations are shorter than the sum of the van der Waals radii. Such heteronuclear Pt−M complexes are shown to

* To whom correspondence should be addressed. E-mail: chenwzz@zju.edu.cn (W.C.), kmatsu@waseda.jp (K.M.), jochena@buffalo.edu (J.A.).
[†] Zhejiang University.
[‡] Waseda University.
[§] University at Buffalo.
[||] University of Calgary.
[⊥] Linköping University.
[#] Royal Institute of Technology.

(1) (a) Hamel, A.; Mitzel, N. W.; Schmidbaur, H. *J. Am. Chem. Soc.* **2001**, *123*, 5106. (b) Codina, A.; Fernández, E. J.; Jones, P. G.; Laguna, A.; López-de-Luzuriaga, J. M.; Monge, M.; Olmos, M. E.; Pérez, J.; Rodriguez, M. A. *J. Am. Chem. Soc.* **2002**, *124*, 6781. (c) Fernández, E. J.; Laguna, A.; López-de-Luzuriaga, J. M.; Monge, M.; Montiel, M.; Olmos, M. E. *Inorg. Chem.* **2005**, *44*, 1163. (d) Stork, J. R.; Rios, D.; Pham, D.; Bicocca, V.; Olmstead, M. M.; Balch, A. L. *Inorg. Chem.* **2005**, *44*, 3466. (e) Catalano, V. J.; Malwitz, M. A. *J. Am. Chem. Soc.* **2004**, *126*, 6560.

10.1021/ic051678o CCC: $33.50
Published on Web 04/25/2006

display luminescent properties. Since the first Pt−Tl complex $[Tl_2Pt(CN)_4]$ was reported by Nagle et al.,[6f] a number of examples of Pt−Tl complexes, including $Pt^{II}-Tl^{I}$,[6] $Pt^{0}-Tl^{I}$,[7] $Pt^{II}-Tl^{II}$,[8] and $Pt^{II}-Tl^{III}$[9] interactions, have been prepared that comprise short Pt−Tl separations.

For many years, we have been interested in the amidate-bridged dimeric Pt complexes of the general formula $[Pt^{III}_2(NH_3)_4(amidate)_2L'L'']^{n+}$ (L′ and L″ are axial ligands) having a Pt oxidation state of 3. These complexes are unique catalysts for selective oxidation of olefins by water O to epoxides or ketones because they exhibit reversible redox behavior between Pt^{III}_2 and Pt^{II}_2 and have two loosely coordinated axial ligands.[10] Such dimeric Pt^{III} compounds were also found to activate C−H bonds of ketones to yield Pt^{III}−ketonyl complexes.[11]

The square-planar Pt^{II} complexes $[Pt(RNH_2)_2(NHCOR')_2]$ may act as soft bases because of the donating ability of the Pt center and the amidate ligands, and thus they may aggregate into heteronuclear complexes with other metal ions by forming Pt−M bonds.[12] While taking into account the oxidation ability of Tl^{III} ions ($E° = 0.33$ V for Tl^{3+}/Tl^{2+}, 2.2 V for Tl^{2+}/Tl^{+}; 1.25 V for Tl^{3+}/Tl^{+})[13] and the metal−metal interactions between Pt and Tl ions,[6−9] it is feasible to obtain heterometallic Pt^{III} or Pt complexes having properties similar to those of the Pt^{III} species stabilized by Pt−Tl interactions. It is noted that oxidation of $[Pt(C_6Cl_5)_4]^{2-}$ by $TlCl_3$ affords paramagnetic Pt^{III} complex $[Pt(C_6Cl_5)_4]^{-}$.[14] Steric hindrance of the four $C_6Cl_5^{-}$ ligands prevents dimerization and aggregation with Tl. Although a number of Pt−Tl complexes have been reported, reactions of Pt^{II} complexes with Tl^{III} ions are scarcely studied and the Pt−Tl cyanide complexes formed by the reaction between $[Pt(CN)_4]^{2-}$ and Tl^{III} species have only recently been described by Glaser's group.[9]

The major goal of this research aims at preparing heteronuclear Pt complexes having Pt^{III}-like centers, which are stabilized by Pt−M bonds and may behave like the known dimeric Pt^{III} complexes. In addition, redox-active coordination complexes are of interest because redox functions expected for the Pt^{III}−M complexes may lead to a variety of intriguing electrical, photophysical, or catalytic phenomena. This also promoted us to study the Pt−Tl complexes possessing two redox-active centers. Continuing our effort to study the properties of the bis(amidate)platinum(II) complexes, we describe herein the synthesis and spectral and structural characterization of the dimeric complex $[\{Pt(ONO_2)(NH_3)_2(NHCO^tBu)\}Tl(ONO_2)_2(MeOH)]\cdot MeOH$ (**2**) and a few trinuclear $[\{PtX(RNH_2)_2(NHCO^tBu)_2\}_2Tl]X$ [X = NO_3^- (**3**), Cl^- (**5**), $CF_3CO_2^-$ (**6**)] complexes. The bonding interactions between Pt and Tl have been studied by multinuclear NMR, UV−vis, and X-ray photoelectron spectroscopy (XPS), and the structures were identified by X-ray diffraction. Spectroscopic data suggest that the Pt oxidation state in these complexes is close to Pt^{III}, which is further supported by the C−H bond activation of acetone to give a platinum acetonate complex, resembling the reactivity of the dimeric Pt^{III} complexes.[11]

Results and Discussion

Synthesis and Structures. When a methanolic (MeOH) solution of 1 equiv of $[Pt(NH_3)_2(NHCO^tBu)_2]\cdot 2H_2O$ (**1**) and $Tl(NO_3)_3\cdot 3H_2O$ is mixed, the colorless solution turns yellow immediately (Scheme 1). Beautiful yellow polyhedral crystals of **2** suitable for X-ray diffraction analysis were grown by

(2) (a) Wong, K. M. C.; Hui, C. K.; Yu, K. L.; Yam, V. W. W. *Coord. Chem. Rev.* **2002**, *229*, 123 and references cited therein. (b) Chen, Y.; Zhang, L.; Shi, L.; Chen, Z. *Inorg. Chem.* **2004**, *43*, 7493. (c) Yam, V. W.-W.; Yu, K.-L.; Wong, K. M.-C.; Cheung, K.-K. *Organometallics* **2001**, *20*, 721. (d) Yamaguchi, T.; Yamazaki, F.; Ito, T. *J. Am. Chem. Soc.* **2001**, *123*, 743.

(3) (a) Balch, A. L.; Fung, E. Y.; Nagle, J. K.; Olmstead, M. M.; Rowley, S. P. *Inorg. Chem.* **1993**, *32*, 3295. (b) Catalano, V. J.; Bennett, B. L.; Noll, B. C. *Chem. Commun.* **2000**, 1413.

(4) (a) Hao, L.; Vital, J. J.; Puddephatt, R. J. *Organometallics* **1996**, *15*, 3115. (b) Catalano, V. J.; Malwitz, M. A.; Noll, B. C. *Inorg. Chem.* **2002**, *41*, 6553. (c) Tanase, T.; Goto, E.; Takenaka, H.; Horiuchi, T.; Yamamoto, Y.; Kuwabara, J.; Osakada, K. *Organometallics* **2005**, *24*, 234.

(5) (a) Fornies, J.; Gomez, J.; Lalinde, E.; Moreno, M. T. *Inorg. Chem.* **2001**, *40*, 5415. (b) Fornies, J.; Ibanez, S.; Martin, A.; Gil, B.; Lalinde, E.; Moreno, M. T. *Organometallics* **2004**, *23*, 3963.

(6) (a) Renn, O.; Lippert, B.; Mutikainen, I. *Inorg. Chim. Acta* **1993**, *208*, 219. (b) Catalano, V. J.; Bennett, B. L.; Muratidis, S.; Noll, B. C. *J. Am. Chem. Soc.* **2001**, *123*, 173. (c) Usón, R.; Forniés, J.; Tomas, M.; Garde, R.; Alonso, P. *J. Am. Chem. Soc.* **1995**, *117*, 1837. (d) Berenguer, J. R.; Forniés, J.; Gómez, J.; Lalinde, E.; Moreno, M. T. *Organometallics*, **2001**, *20*, 4847. (e) Ezomo, O. J.; Mingos, D. M. P.; Williams, I. D. *J. Chem. Soc., Chem. Commun.* **1987**, 924. (f) Nagle, J. K.; Balch, A. L.; Olmstead, M. M. *J. Am. Chem. Soc.* **1988**, *110*, 319. (g) Usón, R.; Forniés, J.; Tomás, M.; Garde R.; Merino, R. I. *Inorg. Chem.* **1997**, *36*, 1383. (h) Stork, J. R.; Olmstead, M. M.; Balch, A. L. *J. Am. Chem. Soc.* **2005**, *127*, 6512. (i) Catalano, V. J.; Malwitz, M. A. *J. Am. Chem. Soc.* **2004**, *126*, 6560. (j) Charmant, J. P. H.; Forniés, J.; Gomez, J.; Lalinde, E.; Merino, R. I.; Moreno, M. T.; Orpen, A. G. *Organometallics* **2003**, *22*, 652. (k) Song, H.; Zhang, Z.; Hui, Z.; Che, C.; Mak, T. C. W. *Inorg. Chem.* **2002**, *41*, 3146. (l) Berenguer, J. R.; Fornies, J.; Gomez, J.; Lalinde, E.; Moreno, M. T. *Organometallics* **2001**, *20*, 4847.

(7) (a) Catalano, V. J.; Bennett, B. L.; Yson, R. L.; Noll, B. C. *J. Am. Chem. Soc.* **2000**, *122*, 10056. (b) Catalano, V. J.; Bennett, B. L.; Muratidis, S.; Noll, B. C. *J. Am. Chem. Soc.* **2001**, *123*, 173. (c) Hao L.; Xiao, J.; Vittal, J. J.; Puddephatt, R. J.; Manojlovic-Muir, L.; Muir, K. W.; Torai, A. A. *Inorg. Chem.* **1996**, *35*, 658. (d) Tanase, T.; Goto, E.; Takenaka, H.; Horiuchi, T.; Yamamoto, Y.; Kuwabara, J.; Osakada, K. *Organometallics* **2005**, *24*, 234.

(8) Usón, R.; Forniés, J.; Tomás, M.; Garde, R. *J. Am. Chem. Soc.* **1995**, *117*, 1837.

(9) (a) Maliarik, M.; Berg, K.; Glaser, K. J.; Sandström, M.; Tóth, I. *Inorg. Chem.* **1998**, *37*, 2910. (b) Berg, K.; Glaser, J.; Read, M. C.; Tóth, I. *J. Am. Chem. Soc.* **1995**, *117*, 7550. (c) Jalilehvand, F.; Maliarik, M.; Sandström, M.; Mink, J.; Persson, I.; Persson, P.; Tóth, I.; Glaser, J. *Inorg. Chem.* **2001**, *40*, 3889. (d) Ma, G.; Fischer, A.; Glaser, J. *Eur. J. Inorg. Chem.* **2002**, 1307. (e) Jalilehvand, F.; Erikson, L.; Glaser, J.; Maliarik, M.; Mink, J.; Sandström, M.; Tóth, I.; Tóth, J. *Chem.—Eur. J.* **2001**, *7*, 2167. (f) Nagy, P.; Toth, I.; Fabian, I.; Maliarik, M.; Glaser, J. *Inorg. Chem.* **2004**, *43*, 5216. (g) Ma, G.; Kritikos, M.; Maliarik, M.; Glaser, J. *Inorg. Chem.* **2004**, *43*, 4328.

(10) (a) Sekiya, H.; Ishihara, K.; Matsumoto, K. *J. Am. Chem. Soc.* **2003**, *125*, 3605. (b) Matsumoto, K.; Nagai, Y.; Matsunami, J.; Mizuno, K.; Abe, T.; Somazawa, R.; Kinoshita, J.; Shimura, H. *J. Am. Chem. Soc.* **1998**, *120*, 2900. (c) Arime, M.; Ishihara, K.; Matsumoto, K. *Inorg. Chem.* **2004**, *43*, 309. (d) Lin, Y.-S.; Takeda, S.; Matsumoto, K. *Organometallics* **1999**, *18*, 4897.

(11) (a) Matsumoto, K.; Matsunami, J.; Mizuno, K.; Uemura, H. *J. Am. Chem. Soc.* **1996**, *118*, 8959. (b) Lin, Y.; Misawa, H.; Matsumoto, K. *J. Am. Chem. Soc.* **2001**, *123*, 569.

(12) (a) Chen, W.; Matsumoto, K. *Inorg. Chim. Acta* **2003**, *342*, 88. (b) Chen, W.; Matsumoto, K. *Eur. J. Inorg. Chem.* **2002**, 2664.

(13) (a) Cotton, F. A.; Wilkinson, G.; Murrillo, C. A.; Bochmann, M. *Advanced Inorganic Chemistry*, 6th ed.; John Wiley & Sons: New York, 1999; p 1083. (b) Khoshtariya, D. E.; Dolidze, T. D.; Zusman, L. D.; Lindbergh, G.; Glaser, J. *Inorg. Chem.* **2002**, *41*, 1728.

(14) Usón, R.; Forniés, J.; Tomós, M.; Menjón, B.; Bau, R.; Süenkel, K.; Kuwabara, E. *Organometallics* **1986**, *5*, 1576.

Scheme 1

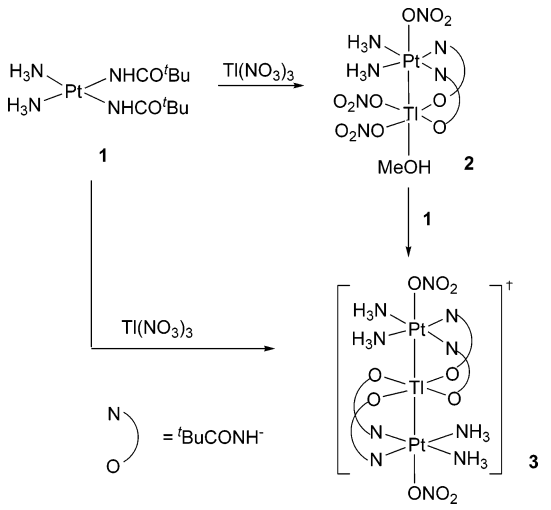

slow evaporation of the yellow solution. Reaction of **1** with $Tl(NO_3)_3 \cdot 3H_2O$ (2:1) in MeOH afforded $[\{Pt(ONO_2)(NH_3)_2(NHCO^tBu)_2\}_2Tl](PF_6)$ (**3**) as greenish-yellow crystals. The complexes **2** and **3** are stable in their solid state in air. They can persist in MeOH and dimethyl sulfoxide (DMSO) for a few days but dissolve in acetone/water to afford a colorless species, which was not identified. Compound **2** is the intermediate in the formation of the trimeric complex **3**, which was confirmed by the reaction of compound **2** with an additional 1 equiv of $[Pt(NH_3)_2(NHCO^tBu)_2] \cdot 2H_2O$ in MeOH, in which compound **3** was readily isolated.

The structures of compounds **2** and **3** are depicted in Figures 1 and 2. The crystallographic data are given in Table 1. Compound **2** consists of $[Pt(NH_3)_2(NO_3)]$ and $[Tl(NO_3)_2(MeOH)]$ moieties bridged by two pivalamidate ligands. The Pt atom coordinates four equatorial N ligands, with an axial NO_3^- ligand and a Tl atom completing the distorted octahedral coordination geometry. The Pt and N atoms around it remain square-planar (the sum of the N−Pt−N angles is 359.9°). The $Pt-O_{nitrate}$ distance [2.288(5) Å] is unusually long, indicative of a strong trans influence exerted by the Pt−Tl bond. The coordination geometry of the Tl ion may be viewed as a severely distorted octahedron. The Tl−O distances (2.295−2.374 Å) are longer than those in $[Tl(H_2O)_6](ClO_4)_3$ [2.23(2) Å],[15a] which has a Tl^{III} center, but much shorter than those in thallium(I) acetylacetate complexes (2.51−2.83 Å)[15b] and thallium(I) anthranilates and salicylates (2.55−2.97 Å).[15c]

The structure of the cation of compound **3** is shown in Figure 2. The complex consists of a perfectly linear Pt−Tl−Pt core. The two $[Pt(ONO_2)(NH_3)_2(NHCO^tBu)_2]$ and a Tl unit are held together by the bridging ligands and the Pt−Tl bonds. The central Tl ion has an octahedral geometry, with two Pt atoms occupying the axial positions and four O atoms on the basal plane. Similar to complex **2**, the main

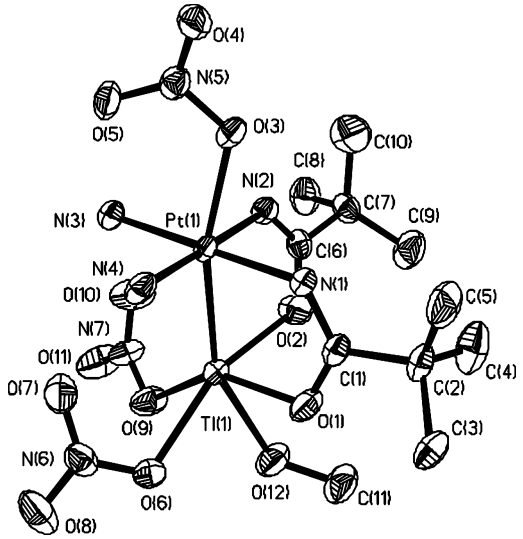

Figure 1. Structure of **2**. Selected bond lengths (Å) and angles (deg): Pt(1)−Tl(1) 2.615(1), Pt(1)−N(1) 2.001(6), Pt(1)−N(2) 1.996(6), Pt(1)−N(4) 2.063(6), Pt(1)−N(3) 2.069(6), Pt(1)−O(3) 2.288(5), Tl(1)−O(6) 2.295(6), Tl(1)−O(2) 2.297(6), Tl(1)−O(12) 2.317(6), Tl(1)−O(1) 2.344(6), Tl(1)−O(9) 2.374(6), N(2)−Pt(1)−N(1) 89.5(2), N(2)−Pt(1)−N(4) 177.2(3), N(1)−Pt(1)−N(4) 89.2(3), N(2)−Pt(1)−N(3) 90.1(2), N(1)−Pt(1)−N(3) 179.4(2), N(4)−Pt(1)−N(3) 91.1(3), N(2)−Pt(1)−O(3) 86.1(2), N(1)−Pt(1)−O(3) 83.0(2), N(4)−Pt(1)−O(3) 91.3(2), N(3)−Pt(1)−O(3) 96.4(2), O(6)−Tl(1)−O(2) 157.6(2), O(6)−Tl(1)−O(12) 79.4(2), O(2)−Tl(1)−O(12) 78.4(2), O(6)−Tl(1)−O(1) 86.5(2), O(2)−Tl(1)−O(1) 93.1(2), O(12)−Tl(1)−O(1) 81.4(2), O(6)−Tl(1)−O(9) 76.4(2), O(2)−Tl(1)−O(9) 93.7(2), O(12)−Tl(1)−O(9) 71.5(2), O(1)−Tl(1)−O(9) 150.1(2).

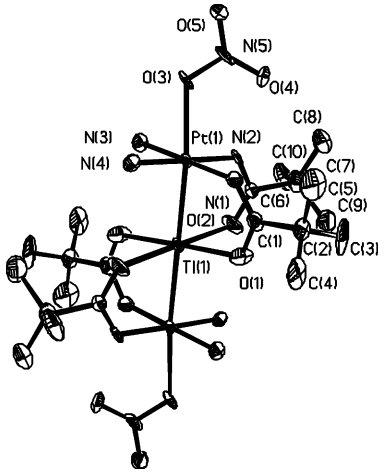

Figure 2. Molecular structure of the trimetallic cation of **3**. Selected bond distances (Å) and angles (deg): Pt(1)−Tl(1) 2.573(1), Pt(1)−N(1) 2.019(13), Pt(1)−N(2) 1.983(13), Pt(1)−N(3) 2.092(12), Pt(1)−N(4) 2.078(13), Pt(1)−O(3) 2.337(11), Tl(1)−O(1) 2.387(11), Tl(1)−O(2) 2.412(12), N(2)−Pt(1)−N(1) 87.4(6), N(2)−Pt(1)−N(4) 177.3(5), N(1)−Pt(1)−N(4) 90.1(5), N(2)−Pt(1)−N(3) 91.2(5), N(1)−Pt(1)−N(3) 178.3(5), N(4)−Pt(1)−N(3), 91.3(5), N(2)−Pt(1)−O(3) 95.2(5), N(1)−Pt(1)−O(3) 97.3(5), N(4)−Pt(1)−O(3) 84.2(5), N(3)−Pt(1)−O(3) 83.7(5), O(1)#1−Tl(1)−O(1) 180.0(11), O(1)−Tl(1)−O(2)#1 91.7(6), O(1)−Tl(1)−O(2) 88.3(6), O(2)#1−Tl(1)−O(2) 180.0(9), Pt(1)−Tl(1)−Pt(1)#1 180.0. Symmetry transformations used to generate equivalent atoms: #1, $-x + 1/2$, $-y + 1/2$, $-z$.

structural feature of **3** is the very short Pt−Tl bond [2.573(1) Å], which is the shortest one among all of the known Pt−Tl bonds.[6−9] The shorter Pt−Tl bonds in **3** are a consequence of the square-planar coordination geometry of TlO_4, which enables a closer approach to the Pt centers than in **2**. The $Pt-O_{nitrate}$ distances are also relatively long because

(15) (a) Ma, G.; Molla-Abbassi, A.; Kritikos, M.; Ilyukhin, A.; Jalilehvand, F.; Kessler, V.; Skripkin, M.; Sandstrom, M.; Glaser, J.; Naslund, J.; Persson, I. *Inorg. Chem.* **2001**, *40*, 6432. (b) Fernández, E. J.; Laguna, A.; López-de-Luzuriaga, J. M.; Monge, M.; Montiel, M.; Olmos, M. E.; Pérez, J. *Organometallics* **2004**, *23*, 774. (c) Wiesbrock, F.; Schmidbaur, H. *J. Am. Chem. Soc.* **2003**, *125*, 3622.

Table 1. Crystallographic Data for Compounds **2**−**6** and **8**[a]

	2	**3**	**4**	**5**	**6**	**8**
formula	$C_{12}H_{34}N_7O_{13}PtTl$	$C_{22}H_{60}F_6N_{10}O_{12}PPt_2Tl$	$C_{48}H_{124}N_{24}O_{36}Pt_4Tl_3$	$C_{24}H_{68}Cl_3N_8O_8Pt_2Tl$	$C_{27}H_{57}F_9N_8O_{11.5}Pt_2Tl$	$C_{14}H_{37}N_5\ O_6Pt$
M_r	883.92	1396.32	3007.18	1297.76	1443.36	566.58
cryst syst	monoclinic	monoclinic	triclinic	triclinic	monoclinic	monoclinic
space group	$P2_1/c$	$C2/c$	$P\bar{1}$	$P\bar{1}$	$P2_1/n$	$P2_1/n$
a, Å	11.593(4)	15.298(12)	11.546(4)	9.734(3)	10.973(3)	6.845(3)
b, Å	20.647(7)	12.938(10)	16.706(6)	11.637(3)	18.383(3)	28.021(12)
c, Å	11.417(4)	23.433(17)	17.045(6)	11.750(3)	24.036(3)	12.533(5)
α, deg	90	90	62.989(6)	74.267(6)	90	90
β, deg	100.012(7)	105.299(12)	75.275(6)	67.206(5)	112.151(3)	105.509(7)
γ, deg	90	90	72.367(6)	78.688(5)	90	90
V, Å^3	2691.0(16)	4474(6)	2764.9(17)	1174.9(6)	4490.6(12)	2316.6(16)
Z	4	4	1	1	4	4
D_{calcd}, Mg/m^3	2.182	2.073	1.806	1.834	2.135	1.625
reflns collected	16903	9959	12463	5692	23607	12859
reflns unique (R_{int})	6152 (0.1124)	3836 (0.0616)	9456 (0.0550)	3924 (0.0406)	9653 (0.0420)	5175 (0.0543)
R1, wR2 [$I > \sigma 2(I)$]	0.0396, 0.0788	0.0734, 0.1994	0.0729, 0.1965	0.0704, 0.1701	0.0648, 0.1828	0.0318, 0.0608

[a] $R1 = \sum||F_o| - |F_c||/\sum|F_o|$. $wR2 = \{\sum[w(F_o^2 - F_c^2)^2]/\sum[w(F_o^2)^2]\}^{1/2}$.

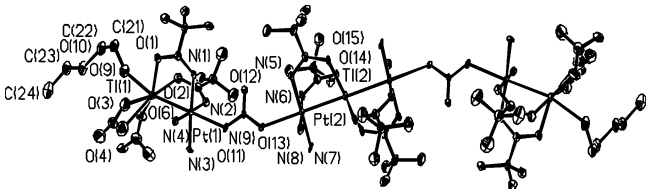

Figure 3. Structure of the cation of **4**. Selected bond distances (Å) and angles (deg): Pt(1)−Tl(1) 2.593(1), Pt(2)−Tl(2) 2.578(1), Tl(1)−O(9) 2.268(16), Pt(1)−O(11) 2.319(11), Pt(2)−O(13) 2.372(12), O(9)−Tl(1)−Pt(1) 164.9(4), O(13)−Pt(2)−Tl(2) 176.7(3), Pt(2)#1−Tl(2)−Pt(2) 180.0. Symmetry code: #1, $-x$, $-y + 2$, $-z$.

of the strong trans effect of the Pt−Tl bonds. The Tl−O distances [2.387(11) and 2.412(12) Å] are longer than those found in **2**. The nitrate anions are weakly coordinated to Pt, as is indicated by the long Pt−$O_{nitrate}$ distances.

When $[Pt(NH_3)_2(NHCO^tBu)_2]$ was reacted with $Tl(NO_3)_3$ in $CH_3CH_2OCH_2CH_2OH$ in a molar ratio of 1:1, a new complex $[\{Pt(NH_3)_2(NHCO^tBu)_2Tl(NO_3)_2(EtOCH_2CH_2OH)\}_2\{\{Pt(NO_3)_2(NH_3)_2(NHCO^tBu)_2\}_2Tl\}](NO_3)_2$ (**4**) was isolated as orange crystals. X-ray analysis revealed that the cation of **4** consists of two dimeric PtTl units and one trimeric Pt_2Tl unit, which are bridged by two NO_3^- ligands. As shown in Figure 3, the two ethoxyethanol molecules are coordinated to the Pt centers of the dimeric PtTl units located at the ends of the molecule via O atoms of the hydroxide groups. The geometrical characteristics observed in the structures of **2** and **3** are also apparent in **4**. All of the structural data including the bond lengths and angles match the corresponding values in **2** and **3**.

Similarly, the reaction of **1** with TlX_3 ($X = Cl^-$, $CF_3CO_2^-$) in a molar ratio of 2:1 yielded the trimetallic complexes **5** and **6** in good yields. Their structures are shown in Figures 4 and 5. The ^{195}Pt NMR spectra of the compounds in MeOH-d_4 indicated that the trimeric species are the sole products, whereas when 1 equiv of $[Pt(RNH_2)_2(NHCO^tBu)_2]$ was employed, both Pt_2Tl and PtTl species were formed. One common feature of the trimeric Pt_2Tl as well as the dimeric complexes is that the axial Pt−X (X = O, Cl) distances are unusually long. The Pt−Cl bond distances of the known Pt^{II} and Pt^{IV} complexes are normally smaller than 2.40 Å, for

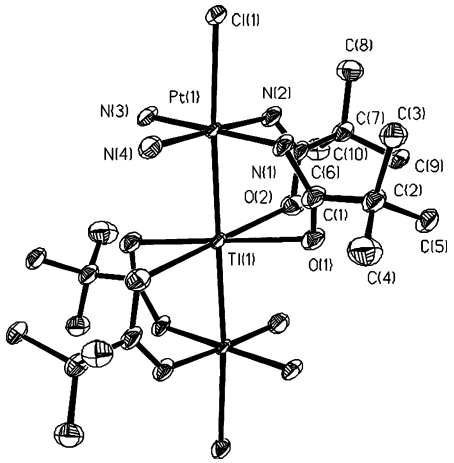

Figure 4. X-ray structural drawing of the cation of **5**. Selected bond distances (Å) and angles (deg): Pt(1)−Tl(1) 2.585(1), Pt(1)−Cl(1) 2.559(5), Tl(1)−O(1) 2.48(7), Tl(1)−O(2) 2.42(2), Cl(1)−Pt(1)−Tl(1) 175.8(1), Pt(1)−Tl(1)−Pt(1)#1 180.0. Symmetry code: #1, $-x + 2$, $-y + 2$, $-z$.

instance, they are 2.316(2)[16] and 2.323(1) Å[17] in K_2PtCl_4 and K_2PtCl_6, respectively. A much longer Pt−Cl_{axial} distance of 2.562(7) Å is found in compound **5**. The Pt−Cl_{axial} distances in some Pt^{III} complexes are 2.407(2) Å in $K_4[Pt_2Cl_2(\mu\text{-}P_2O_5H_2)_4]$,[18] 2.448(4) Å in $(Et_4N)_2[Pt_2Cl_2(\mu\text{-}PO_4H)_2]\cdot H_2O$,[19] 2.444(2) and 2.429(4) Å in $[Pt_2(\mu\text{-}C_5H_4NO)_2Cl_2(NH_3)_4](NO_3)_2$,[20] 2.427(5) Å in $[Pt_2Cl_2(NHCO^tBu)_4]$,[21] and 2.458(3) Å in $[Pt_2Cl_6\{HN{=}C(OH)^tBu\}_4]$.[22] The Pt−$O_{axial}$ bond distances in the nitrate and trifluoroacetate complexes fall in the range of 2.286(5)−2.47(2) Å, which are also much

(16) Mais, R. H. B.; Owston, P. G.; Wood, A. M. *Acta Crystallogr.* **1972**, *B28*, 393.
(17) Williams, R. J.; Dillon, D. R.; Milligan, W. O. *Acta Crystallogr.* **1973**, *B29*, 1369.
(18) Che, C.-M.; Lee, W.-M.; Mak, T. C. W.; Gray, H. B. *J. Am. Chem. Soc.* **1986**, *108*, 4446.
(19) Cotton, F. A.; Han, S.; Conder, H. L.; Walton, R. A. *Inorg. Chim. Acta* **1983**, *72*, 191.
(20) Hollis, L. S.; Roberts, M. M.; Lippard, S. J. *Inorg. Chem.* **1983**, *22*, 3637.
(21) Dolmella, A.; Intini, F. P.; Pacifico, C.; Padovano, G.; Natile, G. *Polyhedron* **2002**, *21*, 275.
(22) Cini, R.; Fanizzi, F. P.; Intini, F. P.; Natile, G. *J. Am. Chem. Soc.* **1991**, *113*, 7805.

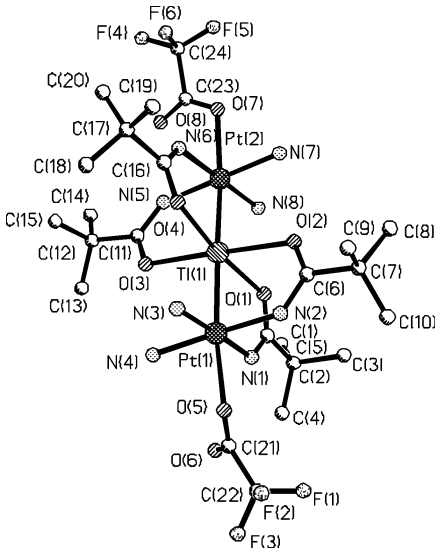

Figure 5. X-ray structure of the cation of **6**. Selected bond distances (Å) and angles (deg): Pt(1)−Tl(1) 2.598(1), Pt(2)−Tl(1) 2.593(1), Tl(1)−O(1) 2.426(8), Tl(1)−O(2) 2.388(8), Tl(1)−O(3) 2.385(8), Tl(1)−O(4) 2.424(8), Pt(1)−O(5) 2.342(8), Pt(2)−O(7) 2.325(7), O(4)−Tl(1)−Pt(1) 98.8(2), O(7)−Pt(2)−Tl(1) 170.0(2), Pt(2)−Tl(1)−Pt(1) 177.29(2).

longer than those in the known Pt^{II} and Pt^{IV} complexes. The Pt−O distances for Pt^{II} and Pt^{IV} complexes are normally around 2.0 Å. The axial Pt−O distances in a few Pt^{III} complexes are 2.279(6) Å for $[Pt_2(H_2O)(PPh_3)(NHCO^tBu)_4](NO_3)_2$,[23] 2.11(1) Å for $[Pt_2(SO_4)_4(H_2O)_2]^{2-}$,[24] and 2.14(1) Å for $[Pt_2(HPO_4)_4(H_2O)_2]^{2-}$.[25]

The $[(NC)_5PtTl(CN)_xL_y]^{-x}$ (L = H_2O, DMSO, 2,2′-bipyridine, 1,10-phenathroline, ethylenediamine, $x = 0-3$, $y = 0-5$) complexes are the only well-characterized Pt−Tl complexes derived from the reaction of Pt^{II} and Tl^{III} compounds.[9] The axial $Pt-C_{cyanide}$ distances in these complexes are essentially identical with those of the equatorial Pt−C bonds. An important structural distinction of the present Pt−Tl complexes from the Pt−Tl cyanide complexes is that the amidate-bridged complexes have quite long $Pt-X_{axial}$ distances, whereas the $Pt-CN_{axial}$ distances are essentially equal to the $Pt-CN_{equatorial}$ distances. The Pt^A atom in the dinuclear $Pt^{III}-Pt^{III}$ complex $[PtCl(NH_3)_2(NHCO^tBu)_2PtCl_3]$[26] (Chart 1) has a coordination environment similar to that of **5**; therefore, it is interesting to compare them. The Pt^A-Cl [2.445(3) Å] and Pt^B-Cl_{axial} [2.400(3) Å] distances are quite close to those of **5**, whereas the two $Pt-Cl_{equatorial}$ distances [2.292(3) and 2.299(3) Å] are normal.

The Pt−Tl bond distances reported in the literature cover a wide range depending on the formal oxidation states: 2.79−3.05 Å for Pt^0-Tl^I,[7] 2.81−3.14 Å for $Pt^{II}-Tl^I$,[6] and 2.70−2.71 Å for $Pt^{II}-Tl^{II}$.[8] The dimeric and trimeric Pt−Tl

Chart 1

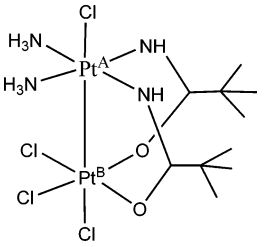

complexes described above have higher total oxidation states and thus shorter Pt−Tl bonds (2.57−2.61 Å). The Pt−Tl bond distances in the present study are comparable to those of $(NC)_5Pt-Tl$ complexes (2.60−2.64 Å), in which the sum of the oxidation states of the two metals is 5.[9]

NMR Characterization in Solution. The ^1H NMR spectrum of **2** in DMSO-d_6 shows the resonance signals of NH, NH_3, and ^{t}Bu at 5.94, 4.68, and 1.31 ppm as singlets, respectively. No coupling between these protons and ^{195}Pt and ^{205}Tl was observed. In the ^1H NMR spectrum of **2**, only one methyl signal was observed corresponding to nearly two molecules of MeOH, illustrating that the coordinated MeOH molecule might be replaced by a DMSO molecule. In MeOH-d_4, the ^{205}Tl NMR spectrum of the bimetallic complex exhibits unusually high-field resonance signals. A singlet with platinum satellites (^{195}Pt, $I = {}^1/_2$, 33.8%) at −874 ppm (intensity ratio 1:3.9:1; $J_{PtTl} = 146\,800$ Hz) for **2** and a five-line pattern centered at −1562 ppm for **3** (intensity ratio close to the ideal 1:7.9:17.4:7.9:1, calculated for the ^{205}Tl NMR spectrum of a trinuclear Pt−Tl−Pt complex considering three possible isotopomers of the compound weighed according to the probability of their occurrence;[9a] $J_{PtTl} = 88\,840$ Hz) were observed, respectively, which are both far outside the usual ranges between −200 and +200 ppm for Tl^I complexes and between +1800 and +3000 ppm for Tl^{III} complexes.[9a] The ^{205}Tl NMR spectra of **2** and **3** are shown in Figure 6.

The ^{195}Pt NMR spectra of the bimetallic compounds in DMSO-d_6 show pairs of doublets due to coupling to two Tl isotopes (^{205}Tl, $I = {}^1/_2$, 70.5%; ^{203}Tl, $I = {}^1/_2$, 29.5%) centered at −980 ppm for **2** and −1133 ppm for **3**, respectively. As expected, the ^{195}Pt NMR spectrum of **4** exhibits two doublets at −1130 ($J_{PtTl} = 89\,002$ Hz) and −851 ($J_{PtTl} = 148\,782$ Hz) assignable to the Pt of Pt_2Tl and PtTl units, respectively, and the chemical shifts and coupling constants are comparable to those of **2** and **3**. The trimeric Pt_2Tl complexes **5**

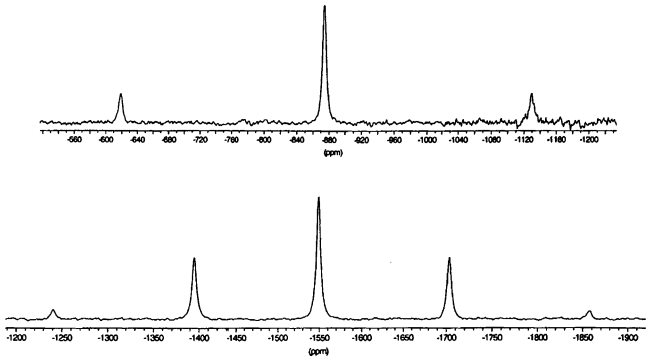

Figure 6. ^{205}Tl NMR spectra of **2** (top) and **3** (bottom) in MeOH-d_4.

(23) Baxter, L. A. M.; Heath, G. A.; Raptis, R. G.; Willis, A. C. *J. Am. Chem. Soc.* **1992**, *114*, 6944.
(24) Bandoli, G.; Dolmella, A.; Intini, F. P.; Pacifico, C.; Natile, G. *Inorg. Chim. Acta* **2003**, *346*, 143.
(25) (a) El-Mehdawi, R.; Fronczek, F. R.; Roundhill, D. M. *Inorg. Chem.* **1986**, *25*, 1155. (b) Cotton, F. A.; Han, S.; Conder, H. L.; Walton, R. A. *Inorg. Chim. Acta* **1983**, *72*, 191. (c) Cotton, F. A.; Falvello, L. R.; Han, S. *Inorg. Chem.* **1982**, *21*, 1709.
(26) Matsumoto, K.; Arai, S.; Ochiai, M.; Chen, W.; Nakata, A.; Nakai, H.; Kinoshita, S. *Inorg. Chem.* **2005**, *44*, 8552.

and **6** show in their ^{195}Pt NMR spectra doublets at −1176 and −1072 ppm, with ^{195}Pt−^{205}Tl coupling constants of 69 101 and 85 518 Hz, respectively. One of the characteristics of all of these complexes is the extremely high value of the Pt−Tl coupling constants, as high as nearly 150 kHz for the dimer **2**. This value is the hitherto highest measured coupling constant between two different nuclei. It is much higher than the previously reported Pt−Tl coupling constants in complexes of Tl^{I}, which are smaller than 7 kHz. So far, the largest known coupling constant between either homo- or heteronuclear atoms is found to be 284.1 kHz for a Hg cluster,[27a] which is due to the large 6s contributions in the metal−metal bonds and the fact that the magnitudes of the valence s-orbital's hyperfine integrals are greatly enhanced by relativistic effects.[27b] Variation of the axial groups X^- seems to have little influence on J_{PtTl} of the Pt−Tl trimeric complexes. All of the ^{195}Pt signals of the Pt_2Tl complexes appear as doublets in a narrow range between −1100 and −1300 ppm, indicating that the Pt electron states are similar. These NMR data show that the ^{195}Pt signals shift downfield from the starting Pt^{II} compounds, and the spin−spin coupling constants of the Pt−Tl complexes are anomalously large because of the intrinsic properties of the two metals. The ^{205}Tl resonance signals of the trinuclear Pt_2Tl compound appear in the high field relative to those of **2**, reflecting the increased electron density at the Tl nucleus upon complexation of the second Pt unit. The coupling constants are larger than those in the Pt−Tl cyanide family; in the latter case, the formal oxidation states of Pt^{II}−Tl^{III} or Pt^{III}−Tl^{II} have been tentatively assigned.[9] The high values of J_{PtTl} have been interpreted in terms of participation of the Tl 6s electrons in the Pt−Tl bond. Because of relativistic effects, the 6s orbital of Tl is stabilized and contracted, which leads to increased electron density at the Tl nucleus and which contributes to the Fermi contact (FC) term for spin−spin coupling. The largest J_{PtTl} reported so far is 94 kHz for $[(NC)_4Pt-Tl(solv)]^+$ in DMSO.[9d] The magnitude of J_{PtTl} in **2** is, to our knowledge, the largest spin−spin coupling constant between two different elements.

Although ^{205}Tl NMR spectroscopy often provides an efficient tool to determine the oxidation state in solution, the ^{205}Tl chemical shifts of **2** and **3** do not match those of most of the known compounds. A few exceptions are also known; for instance, $[Bu_4N][TlI_4]$ gives an extremely high-field signal at −1732 ppm,[28] and Me_3Tl has a chemical shift of 5093 ppm at the other extreme. We are not able to assign the oxidation states of the Tl atom directly from the ^{205}Tl NMR data. They can only be deduced after the oxidation states of Pt are determined. The ^{195}Pt chemical shits of these Pt−Tl complexes lie between those of $[Pt(NH_3)_2(NHCO^tBu)_2]$ (−2429 ppm in DMSO-d_6), typical for the Pt^{II} complex, and *trans*,*cis*,*cis*-$[PtCl_2(NH_3)_2(NHCO^tBu)_2]$ (−35 ppm in DMSO-d_6) and *trans*,*cis*,*cis*-$[PtCl(OH)(NH_3)_2(NHCO^tBu)_2]$ (−134 ppm in DMSO-d_6),[29] typical for Pt^{IV} complexes. The related trinuclear complexes $[\{Pt(NH_3)_2(NHCO^tBu)_2\}_2In](ClO_4)_3$ and $[\{Pt(NH_3)_2(NHCO^tBu)_2\}_2Cd](ClO_4)_2$ show their ^{195}Pt resonances at around −2474 and −2561 ppm, respectively, very close to those of the parent complex $[Pt(NH_3)_2(NHCO^tBu)_2]$, and the oxidation states of the Pt atoms in these Pt_2In and Pt_2Cd complexes are definitely 2.[12b] Thus, it is inferred that the oxidation states of the Pt atoms in the present Pt−Tl complexes are close to 3. The oxidation states of Tl would be between 3 and 1.

A gradual color change in solution from yellow to colorless was observed for these complexes. When the DMSO-d_6 solution of **2** in a NMR tube was kept overnight at room temperature, a new ^{205}Tl resonance signal at −77 ppm and a ^{195}Pt signal at −313 ppm, assigned to Tl^{I} and Pt^{IV} species, respectively, were observed without a ^{195}Pt−^{205}Tl coupling, clearly indicating disruption of the Pt−Tl bonds. The Pt is completely oxidized to Pt^{IV}, and Tl^{III} is reduced to Tl^{I} with cleavage of the Pt−Tl bonds.

XPS. The Pt and Tl 4f core levels of the Pt−Tl complexes as well as a few related Pt complexes were measured with XPS in order to elucidate the oxidation states of the Pt and Tl ions. Actually, in delocalized bonds, assignment of a simple oxidation state is often inappropriate, but the XPS data provide useful information about the real oxidation state. The electron binding energies of **2** and **3** along with those of some known compounds are listed in Table 2.

The Pt 4f core-level spectra of $[Pt(NH_3)_2(NHCO^tBu)_2]$, $[PtCl_2(NH_3)_2(NHCO^tBu)_2]$, **2**, and **3** are shown in Figure 7. The Pt 4f binding energies of $[Pt^{II}(NH_3)_2(NHCO^tBu)_2]$ are very close to that of *cis*-$[Pt^{II}Cl_2(NH_3)_2]$, which are typical Pt^{II} complexes. The Pt 4f binding energy of $[Pt^{IV}Cl_2(NH_3)_2(NHCO^tBu)_2]$ is close to that of $PtCl_4$ (75.5 eV).[30] The XPS spectra of Pt−Tl complexes show that the $4f_{7/2}$ and $4f_{5/2}$ binding energies fall in the narrow ranges of 73.7−74.1 and 76.8−77.3 eV, respectively. These values are also very close to those of $[Pt^{III}_2(NO_3)(NH_3)_4(pyridonate)_2(NO_2)]^{2+}$, whose Pt oxidation states are definitely 3.[31] The electron binding energy depends on the oxidation state of the atom and the local chemical and physical environment. The Pt $4f_{7/2}$ and $4f_{5/2}$ energies of **2**−**6** are nearly equal to the average values of $[PtCl_2(NH_3)_2(NHCO^tBu)_2]$ and $[Pt(NH_3)_2(NHCO^tBu)_2]$ (Figure 7). These data reveal that the oxidation states of Pt in the Pt−Tl complexes are close to 3, which is consistent with the NMR data.

The binding energies of Tl in **2**−**6** appear in the ranges of 118.5−119.0 and 123.0−123.4 eV for $4f_{7/2}$ and $4f_{5/2}$, respectively, which are higher than those of known Tl^{I} and Tl^{III} compounds.[32] The data do not allow us to elucidate the oxidation states of Tl in a straightforward way.

(27) (a) Malleier, R.; Kopacka, H.; Schuh, W.; Wurst, K.; Peringer, P. *Chem. Commun.* **2001**, 51. (b) Autschbach, J.; Igna, C. D.; Ziegler, T. *J. Am. Chem. Soc.* **2003**, *125*, 4937.

(28) Glaser, J.; Henriksson, U. *J. Am. Chem. Soc.* **1981**, *103*, 6642.

(29) *trans*,*cis*,*cis*-$[PtCl_2(NH_3)_2(NHCO^tBu)_2]$ was prepared by dissolving $[Pt(NH_3)_2(NHCO^tBu)_2]$ into a 3% Cl_2 aqueous solution. *trans*,*cis*,*cis*-$[PtCl(OH)(NH_3)_2(NHCO^tBu)_2]$ was preapared by dissolving $[Pt(NH_3)_2(NHCO^tBu)_2]$ into an NaClO aqueous solution. The compounds have been fully characterized by elemental analysis, NMR, and X-ray diffraction analysis.

(30) Escard, J.; Pontvianne, B.; Chenebaux, M. T.; Cosyns, J. *Bull. Soc. Chim. Fr.* **1975**, 2400.

(31) Matsumoto, K.; Sakai, K.; Nishio, K.; Tokisue, Y.; Ito, R.; Nishide, T.; Shichi, Y. *J. Am. Chem. Soc.* **1992**, *114*, 8110.

(32) McGuire, G. E.; Schweitzer, G. K. K.; Carlson, T. A. *Inorg. Chem.* **1973**, *12*, 2451.

Table 2. Electron Binding Energy of the Pt−Tl Complexes

compound	Pt oxidation states	$4f_{7/2}$	$4f_{5/2}$	Tl oxidation states	$4f_{7/2}$	$4f_{5/2}$
$[Pt(NO_3)(NH_3)_2(NHCO^tBu)_2Tl(NO_3)_2(MeOH)]$ (**2**)		74.1	77.2		118.7	123.4
$[\{Pt(NO_3)(NH_3)_2(NHCO^tBu)_2\}_2Tl]^+$ (**3**)		73.7	76.8		118.8	123.2
$[\{PtCl(NH_3)_2(NHCO^tBu)_2\}_2Tl]^+$ (**5**)		74.0	77.3		119.0	123.4
$[\{Pt(CF_3CO_2)(NH_3)_2(NHCO^tBu)_2\}_2Tl]^+$ (**6**)		73.7	77.2		118.5	123.0
trans,*cis*,*cis*-$[PtCl_2(NH_3)_2(NHCO^tBu)_2]$	4	75.3	78.6			
$[Pt(NH_3)_2(NHCO^tBu)_2]$	2	72.3	75.6			
$PtCl_2(NH_3)_2$[a]	2	72.8	76.1			
$[Pt_2(NO_3)(NH_3)_4(pyridonate)_2(NO_2)]^{2+}$ [b]	3	74.6	77.9			
$[Pt_2(en)_2(pyridonate)_2]^{2+}$ [b]	2	73.1	76.4			
$Tl[Pt(CN)_5]$[c]	3.2	74.9		1.6	118.7	
Tl_2O[d]				1	118.5	
Tl_2O_3[e]				3	117.5	

[a] Barton, J. K.; Best, S. A.; Lippard, S. J.; Walton, R. A. *J. Am. Chem. Soc.* **1978**, *100*, 3785. [b] Matsumoto, K.; Sakai, K.; Nishio, K.; Tokisue, Y.; Ito, R.; Nishide, T.; Shichi, Y. *J. Am. Chem. Soc.* **1992**, *114*, 8110. [c] Jalilehvand, F.; Erikson, L.; Glaser, J.; Maliarik, M.; Mink, J.; Sandström, M.; Tóth, I.; Tóth, J. *Chem.—Eur. J.* **2001**, *7*, 2167. [d] Suzuki, T.; Nagoshi, M.; Fukuda, Y.; Syono, Y.; Kikuchi, M.; Kobayashi, N.; Tachiki, M. *Phys. Rev.* **1989**, *B40*, 5184. [e] Sundaresan, A.; Gopinath, C. S.; Tamhane, A. S.; Rajarajan, A. K.; Sharon, M.; Subramanian, S.; Pinto, R.; Gupta, L. C.; Vijayaraghavan, R. *Phys. Rev.* **1992**, *B46*, 6622.

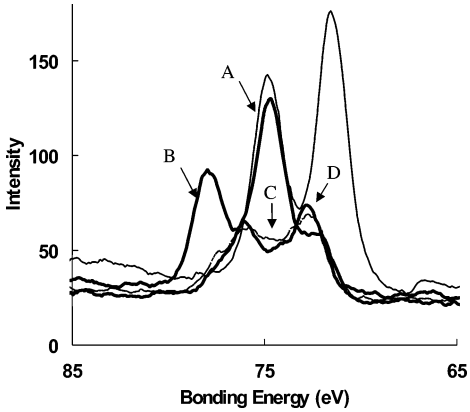

Figure 7. XPS spectra of the Pt 4f core levels of $[Pt(NH_3)(NHCO^tBu)_2]$ (A), $[PtCl_2(NH_3)(NHCO^tBu)_2]$ (B), **2** (C), and **3** (D).

Electronic Absorption Spectra. Because of the instability of the Pt−Tl complexes in solution, all of the UV−vis spectra were measured with freshly prepared solutions just prior to the measurement. The strong covalent Pt−Tl binding interactions are also supported by their UV−vis spectra in solution. The absorption spectrum of the starting Pt complex $[Pt(NH_3)_2(NHCO^tBu)_2]$ shows a band in the UV region at ∼242 nm. The UV−vis spectra of the Pt−Tl nitrate or trifluoroacetate complexes in MeOH solutions show almost identical bands at ∼250 and ∼290 nm. The absorption band at 250 nm closely resembles to that of $[Pt(NH_3)_2(NHCO^tBu)_2]$ and is thus assignable to metal-to-ligand charge-transfer (MLCT) processes. The low-energy 290-nm absorption may arise from the metal-to-metal charge-transfer (MMCT) processes, comparable to the MMCT band at 294 nm of the dinuclear complex $[(NC)_5Pt-Tl(solv)]$ in DMSO.[9] The maximum MMCT band of Pt−Tl−Cl complex **5** in the same solvent was found at 316 nm, which is red-shifted compared to those of the nitrate and trifluoroacetate complexes. Both of the two bands diminished after standing for 2 days at room temperature, indicating the disruption of the Pt−Tl bonds. This is well consistent with the observations of their NMR spectra.

Reactivities toward C−H Activation of Acetone. On the basis of the spectral and structural data analyses, the present

Scheme 2

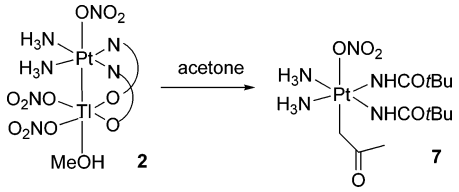

Pt−Tl compounds are believed to resemble the dimeric Pt^{III} complexes. Thus, they are expected to be able to activate C−H bonds of ketones similarly as the pivalamidate-bridged dinuclear Pt^{III} complexes do. This was confirmed by the characterization of the platinum acetonate complex **7** (Scheme 2). The preliminary studies showed that compound **2** reacted with acetone, yielding the acetonylplatinum(IV) complex with simultaneous disruption of the Pt−Tl bond. The Pt center in **2** was oxidized to Pt^{IV}, and the Tl was assumed to be reduced to Tl^{I}, although the Tl-containing product was not identified. Compound **7** was characterized by its ^1H NMR spectrum, which shows a singlet at 3.66 ppm with the coupling constant of $J_{PtH} = 99.2$ Hz.

Because of the difficulty of crystallization of **7**, the platinum(VI) acetonate complex was confirmed by X-ray diffraction analysis of its cyanide analogue $[Pt(CN)(NH_3)_2(NHCO^tBu)_2(CH_2COCH_3)]$ (**8**). As shown in Figure 8, the Pt atom exhibits a typical octahedral geometry. The $Pt-C_{cyanide}$ [2.054(6) Å] bond is normal, whereas the $Pt-C_{acetonyl}$ [2.119(5) Å] bond is somewhat longer. Unlike the amidate-bridged dinuclear Pt^{III} complexes, with which the activation of C−H bonds of ketones always occurs at the Pt centers having a N_2O_2 coordination sphere, the present results show that the Pt having a N_4 coordination environment in the Pt−Tl complex is also active for the C−H bond activation, behaving like the dimeric Pt^{III} complexes.[11]

Computational Results for the Pt−Tl Coupling Constants. The computed Pt−Tl spin−spin coupling constants for complex **2** and the model system **2′** (see the Computational Methods section) are collected in Table 3. All coupling constants are almost exclusively determined by the FC mechanism. The paramagnetic orbital (PSO) mechanism

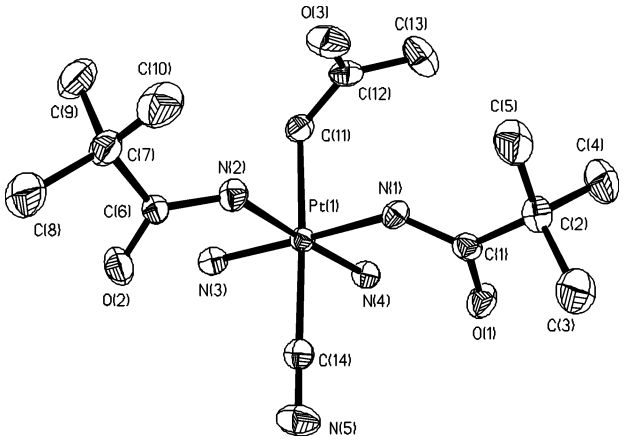

Figure 8. Molecular structure of **8**. Selected bond distances (Å) and angles (deg): Pt(1)−C(14) 2.052(6), Pt(1)−C(11) 2.110(5), Pt(1)−N(1) 2.017(4), Pt(1)−N(2) 2.025(4), Pt(1)−N(3) 2.053(4), Pt(1)−N(4) 2.072(4).

Table 3. Calculated Pt−Tl Spin−Spin Coupling Constants (in kHz) for the Complexes **2** and **2′**[a]

	model A[b] (unsolvated)			model B[c]			model C[d]		
	PSO	FC	total	PSO	FC	total	PSO	FC	total
2[e]	**−0.7**	**114.9**	**114.2**	−0.6	**161.0**	160.3	−0.5	223.4	**222.9**
2′[f]	**−0.7**	**110.4**	**109.7**	−0.6	**156.6**	156.0	−0.5	218.0	**217.5**
2[f]	**−0.7**	**114.9**	**114.2**	−0.6	**159.9**	159.3	−0.5	222.2	**221.7**
2[f,g]	**−1.5**	**125.7**	**124.2**	−1.5	**174.4**	172.9	−1.3	238.1	**236.8**

[a] Couplings refer to ^{205}Tl and ^{195}Pt. The FC + PSO + DSO contributions are included in the scalar relativistic computations. The spin−dipole (SD) contribution is additionally present in spin−orbit computations (included in the listed FC contribution). The DSO contributions are smaller than 0.5 Hz and are therefore not listed. **2′** is a model system with *tert*-butyl replaced by methyl groups. Scalar ZORA computations were carried out unless noted otherwise. [b] Model A: no solvent. [c] Model B: model A + COSMO for the bulk solvent effects. [d] Model C: model B + SAOP. [e] The radii of the atomic spheres used in the COSMO calculations are 1.39, 1.7, 2.2, 1.4, 1.3, and 1.16 Å for Pt, Tl, C, N, O, and H, respectively. $\epsilon = 78.8$ Å (water). [f] The radii of the atomic spheres used in the COSMO calculations are 2.1, 2.4, 2.2, 1.4, 1.3, and 1.16 Å for Pt, Tl, C, N, O, and H, respectively. $\epsilon = 32.6$ (MeOH). [g] Relativistic spin−orbit computations.

contributes only in the order of 1%, while the diamagnetic orbital (DSO) mechanism is completely negligible.

The calculations based on the Vosko−Wilk−Nusair (VWN) functional, without considering solvent effects (model A), underestimate J_{PtTl} by 34 kHz. Nevertheless, the computed coupling constant by far exceeds the magnitudes of the coupling constants for the series of complexes $[(NC)_5Pt-Tl(CN)_n]^{n-}$ (71 kHz for $n = 1$ and decreasing for larger n) and a related system, which were studied computationally by Autschbach and Le Guennic in 2003.[33] Thus, J_{PtTl} for complex **2** represents the hitherto largest computed coupling constant between two different nuclei for an existing stable molecule.

To estimate the possible influence from the environment, solvent effects were further included by means of a continuum model (COSMO, the conductor-like screening model). A rather drastic change of J_{PtTl} results (model B in Table 3), and agreement with the experiment becomes nearly quantitative. The metal−metal coupling constant is thereby not very strongly affected by replacing the *tert*-butyl groups with methyl (**2′**). The difference is only a 2% decrease.

It is interesting to note that the results hardly depend on whether water or MeOH is chosen as the solvent, as compared to the large effect of including either one in the computations. COSMO radii are used to construct the solvent-accessible surface of the molecule. For "inner" atoms that are fully coordinated, we found that the results hardly depend on their radii because they are not accessible by the solvent. Regarding the ligand atoms, we have found in ref 33b that NMR parameters of Pt−Tl bonded complexes also did not change drastically when the COSMO radii were varied within reasonable limits. We expect this to be the case for complex **2** as well.

We have previously found a strong effect from the choice of the exchange-correlation potential on the coupling constants of the complexes $[(NC)_5Pt-Tl(CN)_n]^{n-}$,[33] in particular in conjunction with the COSMO solvent model. Consequently, computations on the systems **2** and **2′** were further carried out with the statistical average of orbital-dependent model potentials (SAOP) applied in addition to the COSMO model. The results are also listed in Table 3 (model C). They now exceed the experimental result by a comparable magnitude as model A underestimates it. It appears that complex **2** is very susceptible to small perturbation of its electronic structure if such pronounced effects of a continuum solvent model and the choice of the XC potential are observed.[34] The overestimation of the spin−spin coupling is not due to a missing treatment of spin−orbit contributions or the SD term because we have carried out a (rather expensive) spin−orbit computation on complex **2**. It is seen that this leads to a further small (compared to the coupling constant's magnitude) but noticeable increase of the coupling. The application of the SAOP leads to a pronounced rearrangement of electronic charge around the metal centers. The calculated Pt/Tl Hirshfeld charges of complex **2** are 0.36/0.43 and 0.37/0.43 for models A and B, respectively, but 0.40/0.57 for model C. The Mulliken charges also increase significantly from model B to C. Overlap populations between the s orbitals of the metals increase strongly from model A to C, which partially rationalizes the increase of the coupling constant. However, the overlap populations reflect only the properties of the unperturbed ground state of the complex in the absence of the nuclear spins and do not consider how effectively its electron spin density can be polarized by the nuclear spins. A full understanding of the trends obtained for different classes of complexes as well as why complex **2** is so susceptible to changes in the computational model needs to consider both ground-state properties and the spin polarizability. A detailed computational study and an analysis of the NMR parameters of complexes **2**, **2′**, and **3** as well as the $[(NC)_5Pt-Tl(CN)_n]^{n-}$ series can be found in ref 49. Here, we summarize the results from this analysis:

Regarding the accuracy of the computed results, we found that the Pt−Tl coupling constant is rather delicately balanced

(33) (a) Autschbach, J.; Le Guennic, B. *J. Am. Chem. Soc.* **2003**, *125*, 13585. (b) Autschbach, J.; Le Guennic, B. *Chem.−Eur. J.* **2004**, *10*, 2581.

(34) Autschbach, J.; Ziegler, T. *Coord. Chem. Rev.* **2003**, *238/239*, 83.

by various competing influences, owing to the sensitivity of the system's properties to small changes in the electronic structure. To obtain better agreement with the experiment for our "best" computational model (C), we believe it would be necessary to further consider a number of explicit solvent molecules and to reoptimize the geometry of the complex including explicit solvation and bulk solvent effects (via the COSMO model). The single-crystal X-ray structure might differ from the solvated complex in small but important details. A preliminary calculation with a partially optimized system at the model A level did, in fact, lead to a smaller coupling constant because of a small change in the Pt−Tl distance. The much larger coupling constant in particular of complex **2** as compared to the previously investigated $[(NC)_5Pt-Tl(CN)_n]^{n-}$ systems has a number of reasons, among these (i) a small highest occupied molecular orbital−lowest unoccupied molecular orbital gap, (ii) large Tl 6s orbital contributions in low-lying unoccupied orbitals, which allow for a very strong spin-density polarization by the nuclear spins in the metal−metal bond, and (iii) the influence from the metal ligands trans to the metal−metal bond. The analysis of the computed coupling constants has shown that a strongly σ-coordinating ligand in this position tends to reduce the metal−metal spin−spin coupling constant. The effect was found to be more pronounced for the $[(NC)_5Pt-Tl(CN)_n]^{n-}$ complexes than for complex **2** and the model system **2′**. For further details, we refer to ref 49.

Summary

The compounds reported here represent new examples of Pt−Tl complexes, which have Pt centers resembling Pt^{III} supported by strong Pt−Tl interaction. Unlike many known $Pt^{II}-Tl^{I}$ complexes, compounds **2**−**4** are not luminescent, neither at room temperature nor at 77 K. They are synthesized easily and are air-stable in their solid state. The Pt oxidation states are close to 3, as evidenced by their ^{195}Pt NMR spectra in solution and the XPS spectra, and are further supported by their structural features revealed by X-ray diffraction analysis in their solid state. The oxidation states of Tl in these complexes cannot be directly assigned. The Tl−O distances in **2** are significantly shorter than those of the trinuclear complexes. All of the Tl−O bond distances are much longer than those in Tl^{III} complexes such as $[Tl(H_2O)_6](ClO_4)_3$[15a] and shorter than those in Tl^{I} complexes.[15b,c] The $M-Tl^{I}-M$ geometry is usually bent as a result of the stereoactive $6s^2$ electron lone pair at the central Tl^{I} ion. A linear conformation is adopted by the present trinuclear Pt_2Tl complexes to allow for maximum electron delocalization. Steric repulsion between the two M units may also force $M-Tl^{I}-M$ to be linear, as found in $Au^{I}-Tl^{I}-Au^{I}$ [1e] and $Pt^{0}-Tl^{I}-Pt^{0}$ [7a] complexes. Therefore, it is quite reasonably believed that the present compounds contain intermediate oxidation states of the two metals and there is a significant covalent component in the Pt−Tl bonds. Although the oxidation state of the metal is not the sole factor to determine the chemical shift, the extremely high-field resonance of the Tl ion is directly indicative of significant shielding arising from electron donation from the Pt $5d_{z^2}$ to the Tl 6s orbital. The formation of covalent Pt−Tl bonds is accompanied by Pt $5d_{z^2}$ electron donation to the Tl 6s orbital, which leads to a decrease of the electron density on Pt and a simultaneous increase of the electron density on Tl^{III}. Because of the formation of strong Pt−Tl covalent bonds for dinuclear and trinuclear complexes, all electrons are paired and thus all compounds are diamagnetic. As a whole, the trinuclear complexes have a Pt oxidation state of close to 3 and appreciable electronic delocalization exists along the Pt−Tl−Pt axis. In this case, collinearity of the trimetallic species is important to allow maximum electronic delocalization, and collinearity of the three metals is actually observed. The formation of strong covalent Pt−Tl bonds explains why the ^{195}Pt resonance appears in the region of Pt^{III} and the Pt 4f binding energies are close to those of Pt^{III}.

As presented above, we assume that the complex $[Pt(NH_3)_2(NHCO^tBu)_2]$ has been oxidized by partly losing its d_{z^2} electron, and the Tl^{III} ion was reduced by gaining electrons filling its 6s orbital, accompanying the formation of covalent metal−metal bonds. The reaction of **2** with additional $[Pt(NH_3)_2(NHCO^tBu)_2]$ leads to further reduction of the Tl species, yielding the trinuclear complex **3**. Each Pt unit contributes two d_z electrons; the four-electron−three-center Pt−Tl−Pt bonds are formed. The characterization of the dimeric and trimeric Pt−Tl complexes in the solid state and in solution indicates that the compounds are supported by very strong Pt−Tl bonds, that is illustrated by short Pt−Tl bond distances in the solid state and extremely large spin−spin coupling constants in solution. The $Pt^{II}-Tl^{I}$ interactions are mostly electrostatic in nature and are believed to be due to the strong Lewis base and acid characters, respectively, of the two metals. However, the Pt−Tl bonds in the present compounds are believed to have covalent character judging from the very large J_{PtTl} values. The bonding interactions between Pt and Tl in these complexes can be best described as covalent coordinative Pt−Tl bonds.

Experimental Section

Materials and Instrumentation. The Pt complex $[Pt(NH_3)_2(NHCO^tBu)_2]$ (**1**) was prepared according to the published procedure from $Pt(NH_3)_2X_2$ ($X = Cl^-$ or I^-).[12a] TlX_3 ($X = NO_3^-$, Cl^-, $CF_3CO_2^-$) and other chemicals were purchased and used as received. Elemental analyses were performed on a Perkin-Elmer PE 2400II analyzer. The ^1H and ^{195}Pt NMR spectra were recorded on a Bruker DMX500 MHz spectrometer. The ^{205}Tl NMR spectra were recorded on a Bruker DMX500 spectrometer at a probe temperature of 298 (±0.5) K. The ^{195}Pt chemical shifts are given relative to aqueous $K_2PtCl_4 = -1630$ ppm, and ^{205}Tl chemical shifts are referred to the signal of an aqueous $TlClO_4$, extrapolated to infinite dilution (0 ppm). The UV−vis spectra were recorded on a Jasco v-570 spectrometer. The XPS spectra were recorded on a JEOL JPS-9010TR spectrometer. Mg Kα radiation operated at 10 kV and 20 mA was used as the X-ray excitation source. The binding energy reported here was corrected by using the C 1s 284.6-eV line observed in the same sample as a reference.

$[\{Pt(NO_3)(NH_3)_2(NHCO^tBu)_2\}Tl(NO_3)_2(MeOH)]\cdot MeOH$ (2). The addition of **1** (47 mg, 0.10 mmol) to a solution of $Tl(NO_3)_3\cdot 3H_2O$ in MeOH (2 mL) immediately resulted in a yellow solution. After standing at 5 °C overnight, compound **2** was collected by

filtration and washed with a small amount of cold MeOH, dried in air. Suitable crystals for X-ray diffraction analysis were obtained by slow evaporation of the MeOH solution. Yield: 69%. Elem anal. Calcd for $C_{11}H_{30}N_7O_{12}PtTl$: C, 15.51; H, 3.55; N, 11.51. Found: C, 15.43; H, 3.20; N, 11.68. ^{1}H NMR (500.00 MHz, DMSO-d_6): δ 5.94 (s, NH, 2H), 4.68 (s, NH_3, 6H), 3.44 (s, CH_3OH, 3H), 1.13 (s, ^{t}Bu, 18H). ^{195}Pt NMR (107.30 MHz, DMSO-d_6): δ −980 (d). ^{205}Tl NMR (CD_3COD): δ −874 (J_{TlPt} = 146 800 Hz).

[{Pt(NO$_3$)(NH$_3$)$_2$(NHCO^{t}Bu)$_2$}$_2$Tl](PF$_6$)·2MeOH (3). The addition of **1** (94 mg, 0.20 mmol) to a solution of $Tl(NO_3)_3{\cdot}2H_2O$ (44 mg, 0.10 mmol) in MeOH (2 mL) immediately yielded a yellow solution. A yellow microcrystalline solid was afforded after the addition of $NaPF_6$ (50 mg). Suitable crystals for X-ray diffraction analysis were obtained by slow evaporation of the filtrate at room temperature. Yield: 87%. Elem anal. Calcd for $C_{20}H_{34}F_6N_7O_{13}PPt_2Tl$: C, 18.03; H, 3.93; N, 10.51. Found: C, 18.22; H, 4.07; N, 10.31. ^{1}H NMR (500.00 MHz, DMSO-d_6): δ 5.71 (s, NH, 4H), 4.74 (s, NH_3, 12H), 3.43 (s, CH_3OH, 6H), 1.08 (s, $C(CH_3)_3$, 36H). ^{195}Pt NMR (107.30 MHz, DMSO-d_6): δ −1133 (d). ^{205}Tl NMR (CD_3OD): δ −1562 (J_{PtTl} = 88 840 Hz).

[{Pt(NH$_3$)$_2$(NHCO^{t}Bu)$_2$Tl(NO$_3$)$_2$(EtOCH$_2$CH$_2$OH)}$_2${Pt(NO$_3$)(NH$_3$)$_2$(NHCO^{t}Bu)$_2$}$_2$Tl}](NO$_3$)$_3$·CH$_3$CH$_2$OCH$_2$CH$_2$OH (4). The compound was prepared similarly to **2**, but ethoxyethanol was used as the solvent and isolated as a yellow solid. Yield: 64%. Elem anal. Calcd for $C_{48}H_{124}N_{25}O_{39}Pt_4Tl_3{\cdot}CH_3CH_2OCH_2CH_2OH$: C, 19.77; H, 4.28; N, 11.08. Found: C, 19.97; H, 4.14; N, 11.78. ^{1}H NMR (500.00 MHz, DMSO-d_6): δ 5.78 (s, NH, 8H), 4.80 (s, NH_3, 24H), 3.53, 3.49, 3.43 (m, CH_2, 12H), 1.16 (t, J_{HH} = 7.0 Hz, 6H), 1.14 (s, $C(CH_3)_3$, 36H). ^{195}Pt NMR (107.30 MHz, DMSO-d_6): δ −1130 (J_{PtTl} = 89 002 Hz), −851 (J_{PtTl} = 148 782 Hz).

[{PtCl(NH$_3$)$_2$(NHCO^{t}Bu)$_2$}$_2$Tl]Cl·4MeOH (5). The compound was prepared similarly to **3** by starting with $TlCl_3$. Yield: 72%. Elem anal. Calcd for $C_{20}H_{52}Cl_3N_8O_4Pt_2Tl$: C, 20.54; H, 4.48; N, 9.58. Found: C, 20.44; H, 4.26; N, 9.26. ^{1}H NMR (500.00 MHz, DMSO-d_6): δ 5.19 (s, NH, 4H), 4.72 (s, NH_3, 12H), 1.05 (s, $C(CH_3)_3$, 36H). ^{195}Pt NMR (107.30 MHz, DMSO-d_6): δ −1176 (J_{PtTl} = 69 101 Hz).

[{Pt(CF$_3$CO$_3$)(NH$_3$)$_2$(NHCO^{t}Bu)$_2$}$_2$Tl](CF$_3$COO)·MeOH·0.5H$_2$O (6). The compound was prepared similarly to **3** by starting with $Tl_2(CF_3COO)_3$. Yield: 46%. Elem anal. Calcd for $C_{26}H_{52}F_9N_8O_{10}Pt_2Tl$: C, 22.27; H, 3.74; N, 7.99. Found: C, 22.20; H, 3.96; N, 8.02. ^{1}H NMR (500.00 MHz, DMSO-d_6): δ 6.16 (s, NH, 4H), 4.74 (s, NH_3, 12H), 1.06 (s, $C(CH_3)_3$, 36H). ^{195}Pt NMR (107.30 MHz, DMSO-d_6): δ −1072 (J_{PtTl} = 85 518 Hz).

[Pt(NO$_3$)(NH$_3$)$_2$(NHCO^{t}Bu)$_2$(CH$_2$COCH$_3$)]·3H$_2$O (7). A few drops of acetone was added to a solution of compound **2** (50 mg) in 2 mL of MeOH. The yellow solution gradually turned to colorless. A microcrystalline solid of **4** was isolated after slow evaporation of the solvents. Yield: 49%. Elem anal. Calcd for $C_{13}H_{31}N_5O_6Pt$: C, 28.47; H, 5.70; N, 12.77. Found: C, 28.22; H, 5.83; N, 12.97. ^{1}H NMR (500.00 MHz, DMSO-d_6): δ 6.49 (s, NH, 2H), 5.36 (s, NH_3, 6H), 3.66 (s, J_{PtH} = 99.2 Hz, CH_2, 2H), 2.06 (s, CH_2COCH_3, 3H), 1.05 (s, $C(CH_3)_3$, 18H). ^{195}Pt NMR (107.30 MHz, DMSO-d_6): δ −532.

[Pt(CN)(NH$_3$)$_2$(NHCO^{t}Bu)$_2$(CH$_2$COCH$_3$)] (8). To a solution of **7** in situ formed as described above was added 2 equiv of KCN in 1 mL of water. Slow evaporation of the solvents gave colorless crystals. Yield: 22%. Elem anal. Calcd for $C_{14}H_{31}N_5O_3Pt$: C, 32.81; H, 6.10; N, 13.67. Found: C, 32.47; H, 6.49; N, 13.97.

X-ray Structure Determination. Data collection was performed on a Bruker Smart CCD diffractometer by using monochromatized Mo Kα radiation, λ = 0.710 73 Å, at room temperature. Data reduction was performed by using the *SAINT*+, version 6.02, software. The data were corrected for absorption by using the program *SADBAS* within the SAINTPLUS package. A direct method was employed to locate Pt and Tl atoms. Subsequent Fourier synthesis gave the remaining non-H atom positions. The H atoms were geometrically fixed and allowed to ride on their attached atoms and were refined with the *XSHELL* software.[35] The final refinement included anisotropic thermal parameters for all of the non-H atoms and converged to the R1 and wR2 values. The crystal data collection and refinement parameters for the compounds are listed in Table 1.

Computational Methods

Density functional theory computations on complex **2** have been carried out with the Amsterdam density functional (ADF) program.[36−37] The nuclear spin−spin coupling constants were calculated with a modified version of the program code described in refs 38 and 39, which is part of the ADF package. Relativistic effects were incorporated in the computations by means of the zeroth-order regular approximation (ZORA).[40−42] All computations were based on the experimentally determined structure. We have employed the VWN local density functional[43] as well as the Kohn−Sham SAOP.[44] The latter has recently been shown to yield improved accuracy of nuclear shieldings.[45] Two of us have further applied this potential to the computations of Pt−Tl spin−spin coupling constants of the complexes $[(NC)_5Pt{-}Tl(CN)_n]^{n-}$ (n = 0−3) and a related system.[33] It has, in conjunction with an appropriate treatment of solvent effects, reproduced the experimental data with good accuracy. Thereby, the combined solvent effects and the influence of the SAOP amount to as much as 80 kHz for the Pt−Tl coupling constant in the n = 1 system, which, in fact, exceeds the magnitude of J_{PtTl} itself (experimental value: 71 kHz). Because of the similarity of the computational problem, we have applied the same strategy here. Solvent effects were included in the present computations by means of COSMO,[46] as implemented in the ADF code.[47] For further details on the computational models and the basis sets, we refer to refs 36, 48, and 49. The applied models are labeled as follows.

(35) Sheldrick, G. M. *SHELX-97, Program for the solution and refinement of crystal structures*; University of Göttingen: Göttingen, Germany, 1997.
(36) Baerends, E. J.; et al. *Amsterdam Density Functional, Theoretical Chemistry*; Vrije Universiteit: Amsterdam, The Netherlands.
(37) te Velde, G.; Bickelhaupt, F. M.; Baerends, E. J.; van Gisbergen, S. J. A.; Fonseca Guerra, C.; Snijders, J. G.; Ziegler, T. *J. Comput. Chem.* **2001**, *22*, 931.
(38) Autschbach, J.; Ziegler, T. *J. Chem. Phys.* **2000**, *113*, 936.
(39) Autschbach, J.; Ziegler, T. *J. Chem. Phys.* **2000**, *113*, 9410.
(40) van Lenthe, E.; Baerends, E. J.; Snijders, J. G. *J. Chem. Phys.* **1993**, *99*, 4597.
(41) van Lenthe, E. The ZORA Equation. Thesis, Vrije Universiteit, Amsterdam, The Netherlands, 1996.
(42) Dyall, K.; van Lenthe, E. *J. Chem. Phys.* **1999**, *111*, 1366.
(43) Vosko, S. H.; Wilk, L.; Nusair, M. *Can. J. Phys.* **1980**, *58*, 1200.
(44) Schipper, P. R. T.; Gritsenko, O. V.; van Gisbergen, S. J. A.; Baerends, E. J. *J. Chem. Phys.* **2000**, *112*, 1344.
(45) Poater, J.; van Lenthe, E.; Baerends, E. J. *J. Chem. Phys.* **2003**, *118*, 8584.
(46) Klamt, A.; Schüürmann, G. *J. Chem. Soc., Perkin Trans. 2* **1993**, 799.
(47) Pye, C. C.; Ziegler, T. *Theor. Chem. Acc.* **1999**, *101*, 396.
(48) Autschbach, J.; Ziegler, T.; van Gisbergen, S. J. A.; Baerends, E. J. *J. Chem. Phys.* **2002**, *116*, 6930.
(49) Le Guennic, B.; Matsumoto, K.; Autschbach, J. *Magn. Reson. Chem.* **2004**, *42*, S99.

Model A: VWN functional, no treatment of solvent effects. Model B: VWN functional + COSMO. Model C: SAOP + COSMO. Because both metals have no open coordination sites, we did not add explicit solvent molecules (MeOH) in the computations. In addition to complex **2**, we have also carried out computations on a smaller model compound **2′**, in which the bulky *tert*-butyl groups have been replaced by methyl groups.

Acknowledgment. J.A. is grateful for support of his research by the National Science Foundation and by the Petroleum Research Fund. This work was supported in part by an Emmy-Noether Fellowship from the Deutsche Forschungsgemeinschaft. W.C. thanks NSFC (Grant 20572096) and Zhejiang provincial NSF (Grant R405066) for support.

Note Added after ASAP Publication. Reference 9d was incorrect in the version published ASAP April 25, 2006. The corrected version was published May 2, 2006.

Supporting Information Available: X-ray crystallographic files in CIF format for compounds **2**−**6** and **8**. This material is available free of charge via the Internet at http://pubs.acs.org.

IC051678O